



HAL
open science

n-ZnO/Out-of-Stoichiometry p-CuCrO₂ Diodes for Efficient and Low-Cost Transparent Electronic Applications

Lorenzo Bottiglieri, Abderrahime Sekkat, Mouncif Belmouhoub, João Resende, Viet Huong Nguyen, Matthieu Weber, David Muñoz-Rojas, Carmen Jiménez, Jean-Luc Deschanvres

► **To cite this version:**

Lorenzo Bottiglieri, Abderrahime Sekkat, Mouncif Belmouhoub, João Resende, Viet Huong Nguyen, et al.. n-ZnO/Out-of-Stoichiometry p-CuCrO₂ Diodes for Efficient and Low-Cost Transparent Electronic Applications. ACS Applied Electronic Materials, 2022, 4 (12), pp.5847-5858. 10.1021/acsaelm.2c01025 . hal-03907057

HAL Id: hal-03907057

<https://hal.science/hal-03907057>

Submitted on 15 Nov 2023

HAL is a multi-disciplinary open access archive for the deposit and dissemination of scientific research documents, whether they are published or not. The documents may come from teaching and research institutions in France or abroad, or from public or private research centers.

L'archive ouverte pluridisciplinaire **HAL**, est destinée au dépôt et à la diffusion de documents scientifiques de niveau recherche, publiés ou non, émanant des établissements d'enseignement et de recherche français ou étrangers, des laboratoires publics ou privés.

n-ZnO/Out-of-stoichiometry p-CuCrO₂ diodes for efficient and low-cost transparent electronic applications

Lorenzo Bottiglieri*¹, Abderrahime Sekkat¹, Mouncif Belmouhoub¹, João Resende², Viet Huong Nguyen³, Matthieu Weber¹, David Munoz Rojas¹, Carmen Jiménez*¹, Jean-Luc Deschanvres*¹

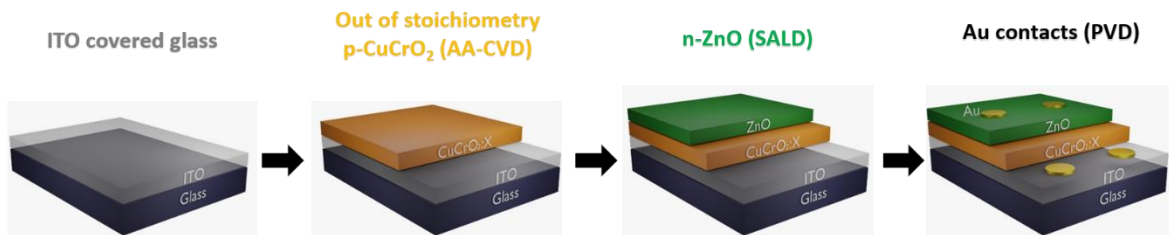
¹ Univ. Grenoble Alpes, CNRS, Grenoble INP, LMGP, F-38000 Grenoble, France

² AlmaScience Colab, Madan Parque, 2829-516 Caparica, Portugal

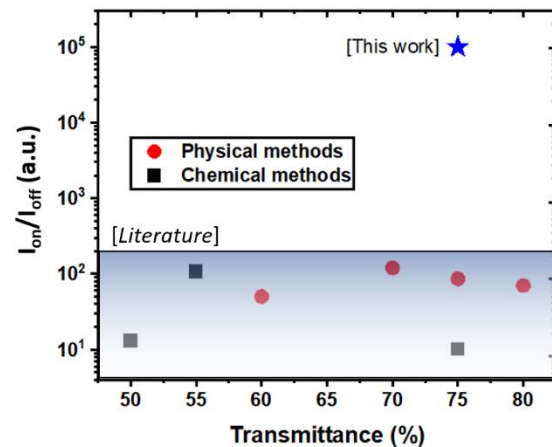
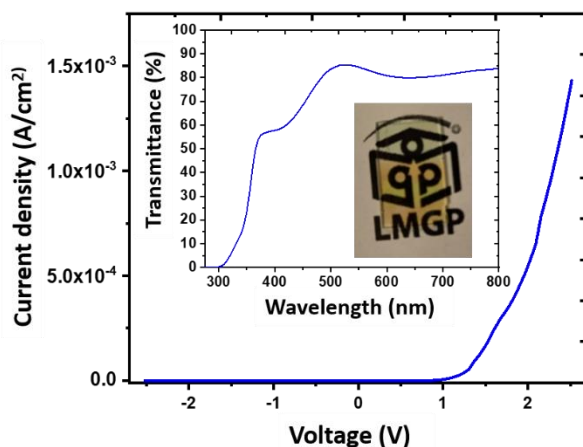
³ Faculty of Materials Science and Engineering, Phenikaa University, Hanoi, Vietnam.

ABSTRACT: In this work, we present the synthesis of high-performance transparent diodes based on p-type out of stoichiometry CuCrO₂ and n-type ZnO thin films. The oxides were fabricated by scalable chemical deposition methods at low temperature and ambient pressure, without any further post-deposition annealing treatment. We report the optimization of the devices through the fine-tuning of the deposition parameters of the two layers, namely, the composition of the p-type semiconductor and the deposition temperature of the n-type counterpart, and their thorough characterization. UV-VIS spectroscopy measurements highlighted the antireflection function of the ZnO layer, resulting in a transmittance of the junction above 75% in the visible range. In-depth XPS profile studies confirmed the absence of atomic diffusion between the different layers. The optimized junction between a nanocomposite Cu₂O+CuCrO₂ coupled with polycrystalline ZnO presents the highest rectification ratio reported in the literature for similar devices, with values greater than 10⁵ between -2.5 V and +2.5 V. These extremely high performances are attributed to the formation of intraband levels, due to the stoichiometry variation of the CuCrO₂ phase and the low crystallinity of n-type ZnO. These results open many prospects for optoelectronics and are particularly promising for the transparent oxide electronics industry.

Keywords: chemical deposition methods, transparent electronics, transparent p-n junctions, MOCVD, Spatial ALD, thin films



Fabrication of planar p-n junctions a low T and ambient pressure



1. Introduction

The production of transparent and performant all-oxide p-n junctions fabricated through low-cost processes represent one of the greatest challenges for the transparent electronics industry. The versatility of such devices, which can be applied as diodes, photo detectors^{1,2}, transparent solar cells³⁻⁵, and light-emitting diodes⁶, justifies the growing interest in this field. Various metal oxides have been integrated as active and passive components in the previously mentioned devices. In this framework, one of the limiting factors is the lack of highly conductive p-type transparent conductive oxides (TCOs) and issues related to the low energy of the valence bands⁷. Among promising p-type oxide semiconductor materials, Cu₂O⁸ and NiO⁹ were successfully applied in optoelectronic devices¹⁰⁻¹². Nevertheless, they suffer from various limitations, hindering their widespread application. For instance, Cu₂O presents limited transparency, with a corresponding bandgap around 2.2 eV¹³, whereas NiO is characterized by a small carrier mobility^{14,15}. Therefore, more research efforts are required to obtain novel more efficient p-type TCOs.

CuCrO₂ is considered a promising p-type TCO for efficient p-n junctions due to its relatively high conductivity, around 1 Ω.cm for the stoichiometric compound¹⁶, and good transparency, around 70% in the visible range¹⁶. Various deposition methods have been used for its synthesis, such as pulsed laser deposition (PLD)¹⁷, RF magnetron sputtering¹⁸, metal-organic chemical vapor deposition (MOCVD)¹⁹⁻²¹, spray pyrolysis²²⁻²⁵ (SP), atomic layer deposition (ALD)¹⁶, sol gel^{26,27}, and hydrothermal synthesis²⁸. Different reports highlighted the enhancement of the optical and electrical properties of CuCrO₂ by tuning the stoichiometry of this material^{19,23,29,30}, with the lowest resistivity among non stoichiometric films, around 0.01 Ω.cm, achieved for Cu-poor compounds, Cu_{0.66}Cr_{1.33}O₂, synthesized by dynamic liquid-injection MOCVD (DLI-MOCVD)³¹. Furthermore, previous works reported the successful integration of this material in a wide range of applications such as organic³², perovskite^{33,34}, and dye-sensitized solar cells^{35,36}, photodetectors³⁷⁻³⁹, gas sensor^{40,41}, photocatalytic devices⁴², and Q-switched fiber laser⁴³.

ZnO is considered a promising n-type TCO for transparent electronics⁴⁴⁻⁴⁶ owing its wide direct band gap, around 3.4 eV, its high electron mobility, around 200 cm²V⁻¹s⁻¹⁴⁷, together with the possibility to be synthesized at low temperature using solution-based and other soft scalable methods⁴⁸⁻⁵⁰. The coupling of p-CuCrO₂ with n-ZnO has been previously reported for the fabrication of transparent diodes⁵¹. To evaluate the electrical performances of these devices, the rectification ratio (I_{on}/I_{off}) is generally considered to be a fundamental criterion. This parameter is defined as the ratio between the current measured at positive voltage, and the one measured at negative bias. On one hand, various works reported the deposition of such devices by physical deposition methods, employing either high temperatures or low pressure, and generally requiring a post-deposition treatment. The transparent p-n junctions fabricated using such techniques showed a rectification ratio, I_{on}/I_{off} , with the highest value ever reported being 120 at ± 5 V⁵². On the other hand, different works reported the fabrication of CuCrO₂/ZnO-based p-n junctions by chemical routes and a summary of the obtained results is reported in Table 1. The use of solution-based processes implies various fabrication advantages, such as the reduction of the used deposition temperature, ambient pressure and affordable surface scalability⁵³, both promising aspects for the industrialization of such devices. Nevertheless, the rectification ratio obtained is one order of magnitude lower than for physical deposition methods. The other chemical approaches reported (MOCVD and SP) involve high deposition temperatures and again the rectification ratios obtained are lower than for diodes obtained by physical deposition methods. Thus, there is a need to develop new chemical processes at low temperature yielding high rectification ratios for diodes based on ZnO and CuCrO₂.

Table 1 Summary of the productive steps reported in the literature for the fabrication of CuCrO₂ and ZnO-based heterojunctions. The reported information are the CuCrO₂ and ZnO technique and growth temperature, the structure of the device, used annealing

conditions (here '/' corresponds to no annealing step, TA corresponds to Thermal annealing, RT corresponds to room temperature, while NR stands for not reported), and the reference.

CuCrO ₂		ZnO		Structure	Annealing	Rectification ratio (I _{on} /I _{off})	Average transmittance in visible(%)	Reference
Growth technique	Growth temperature (°C)	Growth technique	Growth temperature (°C)					
Spin coating	RT	Spin coating	RT	CuCrO _{2+x} /ZnO	TA 180°C 10 min	NR	>70	32
DLI-MOCVD	450	ALD	150	Cu _{0.66} Cr _{1.33} O ₂ /ZnO	TA 700°C 15 min	-4 to +4 V 13	50	54
SP	500	SP	400	ZnO/CuCrO ₂	/	107	55	55
SP	450	LP-CVD	400	CuCr _{0.93} Mg _{0.07} O ₂ /ZnO	/	10	75	56

In our previous work²⁹, we investigated the effect of the cationic ratio i.e. Cu/(Cu+Cr) over the properties of the films CuCrO₂ and we observed enhanced functional properties for Cu-rich CuCrO₂ film with an optimal film composition in the 60 – 70% range, named out of stoichiometry films from now on. Thus non stoichiometric films and nanocomposite films, consisting in a mixture of Cu₂O and CuCrO₂ phases, were obtained by aerosol-assisted metal-organic chemical vapour deposition⁵⁷ (AA-MOCVD), thus with no vacuum being involved, at only 350° C and showed an optical transmittance of around 55% and resistivity values of 0.1 Ω.cm for film with a composition Cu/(Cu+Cr) of 63%²⁹. In the literature there are few reports about the integration of non-stoichiometric CuCrO₂ for diode applications. Only Afonso et al.⁵⁴ reported the application of Cu_{0.66}Cr_{1.33}O₂ in these devices, however the obtained rectification ratio is extremely poor, around 13, achieved only after thermal annealing at high temperature, 700 °C, incompatible with the majority of glass substrates.

In this work, we aimed to investigate the feasibility of this p-type semiconductor for diode application. Out of stoichiometry CuCrO₂ thin films were coupled with ZnO layers synthesized using atmospheric pressure spatial atomic layer deposition⁵⁸ (AP-SALD, a faster, more scalable approach to ALD⁵⁹) to fabricate planar heterojunctions using low-temperature (≤ 350 °C) and scalable methods and without any post-deposition treatment. An ITO covered glass was selected as substrate for its suitability for industrial applications. The properties of the p-type TCO were tuned through the control of its stoichiometry and correlated to the performance of the heterojunctions. Besides, the effect of the deposition temperature of the ZnO thin film was also investigated. The optimized devices show a record-breaking I_{on}/I_{off} ratio, evaluated between -2,5V and 2.5V, with a high transparency in the visible.

2. Material and methods

2.1 Device fabrication

Out of stoichiometry CuCrO_2 thin films were synthesized on borosilicate glass (Corning glass 1737) and ITO-covered glass (Delta technologies CG-51IN-S115) using AA-MOCVD. Films deposited on Corning glass 1737 were used as references, while the ones deposited on ITO were used for the fabrication of the devices. The initial solution was composed of chromium (III) acetylacetonate ($\text{CrC}_{15}\text{H}_{21}\text{O}_6$ by Sigma Aldrich) and copper (II) acetylacetonate ($\text{CuC}_{10}\text{H}_{14}\text{O}_4$ by Strem Chemicals) in ethanol, with a total molar concentration fixed at 10 mM. The Cu partial molar concentration in the solution i.e. $\frac{[\text{Cu}(\text{acac})_2]}{([\text{Cu}(\text{acac})_2]+[\text{Cr}(\text{acac})_3]}$, in the following X, was varied from 50% to 80%. The choice of this concentration range is based on our previous work²⁹, and yields CuCrO_2 thin films with the best optical-electrical properties. Ethylenediamine ($\text{C}_2\text{H}_8\text{N}_2$, Sigma Aldrich), with a concentration of 20 mM, was added to improve the solubility of the precursors in the solvent used. During the deposition, the temperature of the substrates was set to 350 °C. Dried compressed air was used as reactive and carrier gasses with a total flow rate of 4000 sccm. Further information about the used reactor can be found somewhere else²⁹. For the device's fabrication, CuCrO_2 films were deposited over a 1.5 x 1.5 cm² area on the ITO covered glass.

The ZnO thin films were simultaneously deposited on corning glass 1737, used as references, and on top of the ITO/ CuCrO_2 structures on a surface of 0.75 cm² by using a shadow mask employing a custom-built SALD system⁶⁰. The distance between the substrate and the SALD injection head was approximately 150 μm with a scanning speed of 10cm/s. Diethylzinc precursor (C_2H_5)₂Zn (DEZ) was used to deposit ZnO, using a flow of 30 sccm with 150 sccm of H_2O , respectively diluted in 270 and 300 sccm of N_2 . The N_2 barrier total flow was 900 sccm. The deposition temperature was varied between 100 °C, 150 °C, and 200 °C. The number of ALD cycles was varied ensuring similar ZnO thicknesses at different deposition temperatures. The devices were completed by depositing circular Au contacts by thermal evaporation using an EDWARDS FTM6 evaporator, with a current of 4 A for 3 minutes, keeping the chamber pressure at 1×10^{-5} Pa. The effective area of the final devices was around 0.04 mm².

The electrical properties of the individual layers were measured by the linear 4-probe method, through at least 5 testing points to obtain an average value for the sheet resistance. The room temperature transport properties of the materials were obtained with a Hall-effect system using a magnetic field of 0.5 T. X-ray diffraction (XRD) patterns were obtained using a Bruker D8 Advance diffractometer in Bragg-Brentano configuration (θ - 2θ) with Cu $\text{K}_{\alpha 1}$ radiation ($\lambda=1.54 \text{ \AA}$).

2.2 Device characterization

Raman spectroscopy was performed at room temperature with a Jobin Yvon/ Horiba LabRam spectrometer equipped with a liquid nitrogen-cooled charge-coupled detector. Raman spectra were collected in the 50–1000 cm^{-1} frequency range. A blue laser with a wavelength of 488 nm and a power of 0.4 mW at the sample surface was focalized for 10 min to obtain these spectra. This characterization was performed by using a spot size of around 1 μm^2 obtained by using a 100 \times objective.

Grazing Incidence X-ray Diffraction (GIXRD) acquisitions were collected at the range 20-70° with a step of 0.06° on a RIGAKU Smartlab equipped with a 9-kW rotating anode Cu source (45 kV and 200 mA). TEM cross-section observations were performed to measure the thickness of the films on a JEOL 2010 LaB6. Selected area diffraction (SAED) was performed on the same apparatus. For this characterization, the devices were prepared by the formation of a substrate/device/glue/device/substrate architecture, followed by mechanical polishing and Argon gun sputtering until the perforation of the interface.

The optical properties of the devices were analyzed through UV-VIS-IR spectroscopy on a Lambda 950 spectrophotometer from Perkin Elmer equipped with an integrated sphere, using a wavelength step of 5 nm in the 250 to 1000 nm range. Depth-profile X-ray photoelectron spectroscopy (XPS) measurements were

used to evaluate the chemical composition of the device. The C 1s, Zn 2p, Cu 2p, Cr 2p, and O 1s energy regions were scanned using a K-alpha spectrometer from Thermo Fisher Scientific equipped with an Al X-ray source (1486.6 eV). A Depth profile analysis was carried out by measuring after successive 30 s Ar etchings (2 keV).

Current-voltage measurements were made using tungsten tips connected to a Keithley 2400 source meter, sweeping the voltage among ± 2.5 V with a step of 0.06 V, and recording the corresponding current. A minimum of three diodes were tested for each configuration, with a minimum of two measurements for each device. The diode parameters were extracted using 2-3 Diode Fit software by nano-HUB, following the classic diode equation:

$$I = I_0 \left(e^{\frac{q(V-IR_s)}{\eta k_B T}} - 1 \right) + \frac{V - IR_s}{R_{sh}}$$

with I being the current (A), I_0 being the reverse current (A), q being the elementary electronic charge, V corresponding to the external bias voltage, R_s being the series resistance ($\Omega \cdot \text{cm}^2$), n being the ideality factor, k_B being the Boltzmann's constant, T being the absolute temperature in kelvin, and R_{sh} being the shunt resistance ($\Omega \cdot \text{cm}^2$).

3. Results

The electrical and optical properties of CuCrO_2 and ZnO thin films synthesized on Corning glass as reference are presented in

Table 2. The values for CuCrO_2 films were obtained experimentally whereas the values for ZnO layers are extracted from previous experiments in our group⁴⁸ and validated by the repetition of these experiments. As previous found²⁹, the at.% of Cu in the CuCrO_2 films has an impact on the different properties: an increase in Cu ratio initially shows a reduction of the electrical resistivity of the thin films, presenting a minimum for samples synthesized by an initial solution composition of 70%. Increasing further the Cu ratio makes resistivity increases abruptly by 1.5 orders of magnitude and an enhancement of carrier mobility. The band gap shows a monotonical decrease with increasing Cu content.

Table 2 Electrical and optical properties for out of stoichiometry CuCrO_2 and ZnO films on glass. The information reported is the electrical resistivity (ρ), the carrier mobility (μ), charge carrier density (N), and energy gap (E_g) for the two materials deposited under the different conditions. In this table, 'NR' stands for not reliable corresponding to the experimental impossibility of measuring the transport properties of certain materials.

CUCRO₂				
Cu/(Cu+Cr) in the solution (%)	ρ ($\Omega \cdot \text{cm}$)	μ ($\text{cm}^2 \cdot \text{V}^{-1} \cdot \text{s}^{-1}$)	N (cm^{-3})	E_g (eV)
50	1	< 0.1	NR	3.2
60	0.1	< 0.1	NR	3.05
70	0.08	0.9	1×10^{20}	2.9
80	1.2	1.1	8×10^{19}	2.6

ZnO				
Deposition temperature (°C)	ρ ($\Omega\cdot\text{cm}$)	μ ($\text{cm}^2\cdot\text{V}^{-1}\cdot\text{s}^{-1}$)	N (cm^{-3})	Eg (eV)
100	1.5×10^4	NR	NR	3.5
150	0.32	0.5	2.6×10^{19}	3.4
200	0.05	3.2	4.5×10^{19}	3.3

The effect of the stoichiometry on the performance of the devices was probed by varying the Cu/(Cu+Cr) in the initial solution. The diodes will be defined as $\text{CuCrO}_2\text{:X}$, where X represents the % of Cu in the initial solution from which the films have been obtained. The ZnO layers were deposited at 100 °C in all cases.

The XRD patterns of $\text{CuCrO}_2\text{:X}$ films are reported in Figure 1.a) and were compared with the ICDD reference of the delafossite rhombohedral CuCrO_2 structure (ICDD 04-010-3330) and cubic Cu_2O (ICDD 00-005-0667). These results confirm the presence of CuCrO_2 thanks to the (012) and the (110) reflection at $2\theta=36.4^\circ$ and $2\theta=62.4^\circ$ associated to the CuCrO_2 phase. For the two highest compositions i.e., X=70% and X=80%, the formation of the Cu_2O is proved by the appearance of the reflection (200) at $2\theta=42^\circ$. These results are in good agreement with our previous works^{29,57}. A schematic diagram of the device structure is visible in Figure 1.b). The ohmic contact between the probes and the various layers that make up the device were confirmed by the linear characteristic of the Au/ITO/ CuCrO_2 /Au and Au/ITO/ZnO/Au structures, Figure S1.

The effect of varying the CuCrO_2 stoichiometry, X, over the electrical performances of these diodes is reported in Figure 1.c). The limited electrical properties of the integrated TCOs allowed us to consider the effective surface of the device that of the size of the used electrodes and a negligible lateral conductivity.

All the fabricated devices present a rectification ratio, with a value of $I_{\text{on}}/I_{\text{off}} (\pm 2.5\text{V}) \geq 1000$, regardless the composition of CuCrO_2 used. Furthermore, these measurements confirm the p-type conductivity of CuCrO_2 synthesized by an initial solution of 50% and 60%, which was challenging to confirm by Hall Effect measurement, due to the moderate magnetic field in our system. This demonstrates the successful applicability of these thin films as p-type semiconductor for diode applications. The electrical noise found in the J-V characteristic of the $\text{CuCrO}_2\text{:60\%}$ and $\text{CuCrO}_2\text{:70\%}$ devices is attributed to the extremely low reverse bias current, in the order of pA, below the system detection limit. The best performances were obtained for $\text{CuCrO}_2\text{:70\%}$ devices with a corresponding $I_{\text{on}}/I_{\text{off}} (\pm 2.5\text{V})$ around 10^5 . This is mainly attributed to the reduction of the current under reverse polarization.

The trend of $I_{\text{on}}/I_{\text{off}}$ ratio with the composition of the initial solution is confirmed by the statistical analysis of several devices deposited on different samples in the same deposition conditions, Figure 1.d), where a minimum of 3 diodes were tested. The reproducibility of these results obtained for the most performant device was also validated through the fabrication of 4 different samples using the same conditions, Figure S2. Despite the variability of the performances, the devices $\text{CuCrO}_2\text{:70\%}$ always showed a rectification ratio

greater than 10^4 , Figure S2, two orders of magnitude higher than similar devices reported previously in the literature^{52,55}.

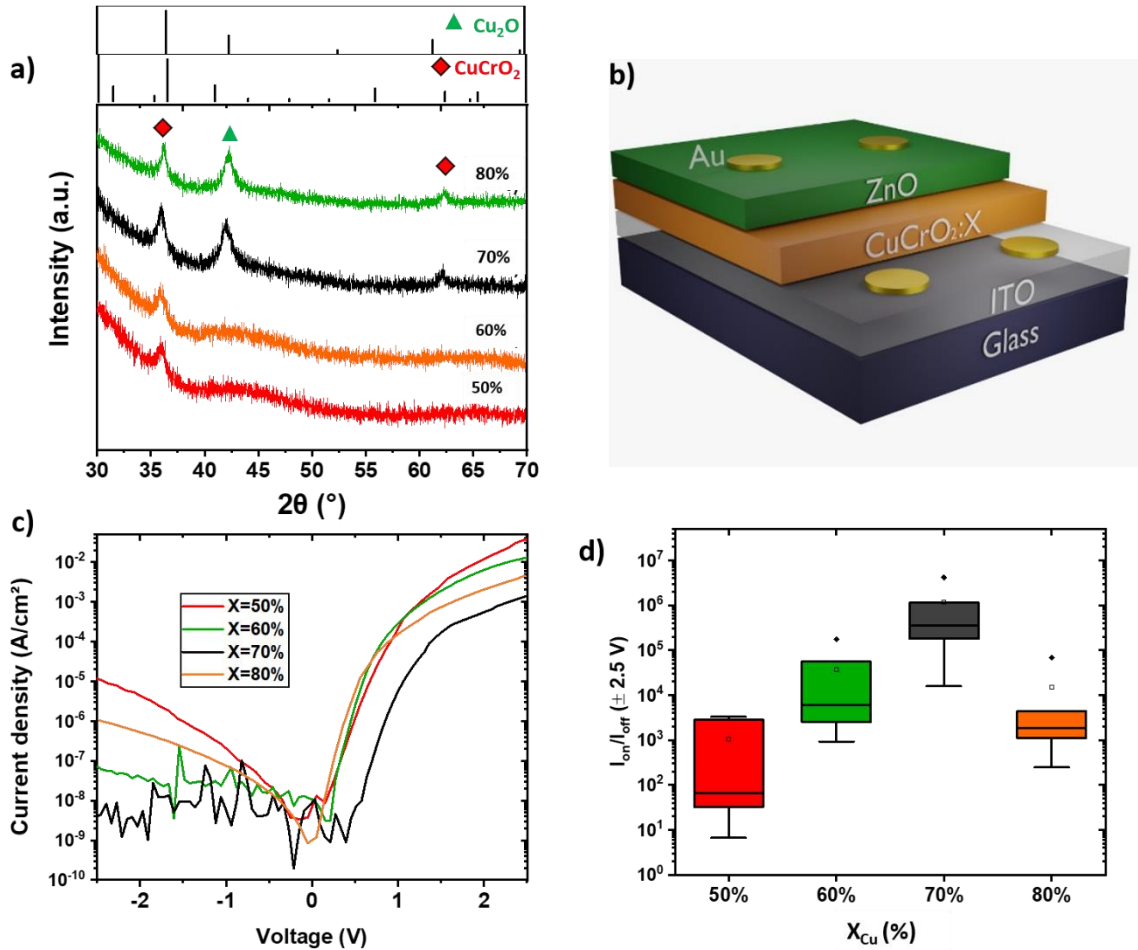


Figure 1. a) XRD patterns of out of stoichiometry CuCrO₂ thin films synthesized on glass by a value of X (solution concentration) of 1) 50%, 2) 60%, 3) 70% and 4) 80%. The CuCrO₂ phase is identified by the reflection (012) at 36.4° and the Cu₂O by the reflection (200) at 42°. b) Schematic architecture of diodes with CuCrO₂ as p-type TCOs, indicated as CuCrO₂:X and ZnO as n-type. c) J-V characteristics in dark for the CuCrO₂:X devices for ZnO deposited at 100°C. d) Box chart of the I_{on}/I_{off} calculated from the J-V characteristics obtained by at least 3 diodes deposited in different samples. The percentiles are set to 95% whisker top, 75% box top, 25% box bottom, and 5% whisker bottom for each data set. The solid and empty squares represent the outliers and the mean, respectively.

Based on these results, CuCrO₂:70% was chosen to further improve the devices by optimizing the n-type ZnO layer. In particular, the deposition temperatures and thickness for ZnO was varied. Increasing the deposition temperature from 100 to 200 °C results in a reduction of the resistivity, through a simultaneous increase of the mobility and carrier density (

Table 2). The increase in the deposition temperature also leads to a reduction in the energy gap. Finally, the deposition temperature modifies the structural properties of the films, as visible in Figure 2.a). The ZnO films deposited at 100 °C show a poor crystallinity, while films deposited at 150 and 200 °C show an increasing crystallization and a texture change towards the (002) direction, according to ICDD 00-036-1451. For a deeper insight into the effect of the various deposition parameters involved in this work, refer to our previous publications on ZnO⁴⁸. The effect of the ZnO deposition temperature on the characteristic of the

diodes is reported in Figure 2.b). The highest rectification ratio is achieved for device where the ZnO film was deposited at 100°C.

Furthermore, we can observe a shift of the origin of the curves, as visible in Figure 2.b). This can be justified by the presence of recombination centers at the interface. We observe that the origin of the J-V characteristic tends towards the zero-bias value, when increasing the deposition temperature of ZnO. This is coherent with the fact that a greater deposition temperature would reduce the presence of impurities i.e., recombination centers at the interface which may work as dipoles thus resulting in charge accumulation and the shift of the curves.

The effect of the thickness of the ZnO layer deposited at 100° C was also investigated, Figure S3. We used 160 ALD cycles to deposit a 30 nm thick ZnO film, and 320 ALD cycles for a 60 nm thick ZnO film, maintaining the other parameters constants. The obtained rectification ratio, for the thinner layer, around 4200, is lower than for the thicker ZnO film, due to a reduction of the forward current. This may be attributed to a greater presence of recombination centers for the thinner film, resulting in increased carrier recombination at the interface and finally limiting the current in the ON state. Hence, the best results were obtained for the combination of CuCrO₂ synthesized by X=70% and a 60 nm thick ZnO film deposited at 100 °C, summarized as ITO/CuCrO₂:70%/ZnO-100°C-320 cycles. The impact of the thickness of the CuCrO₂ will be source of further studies.

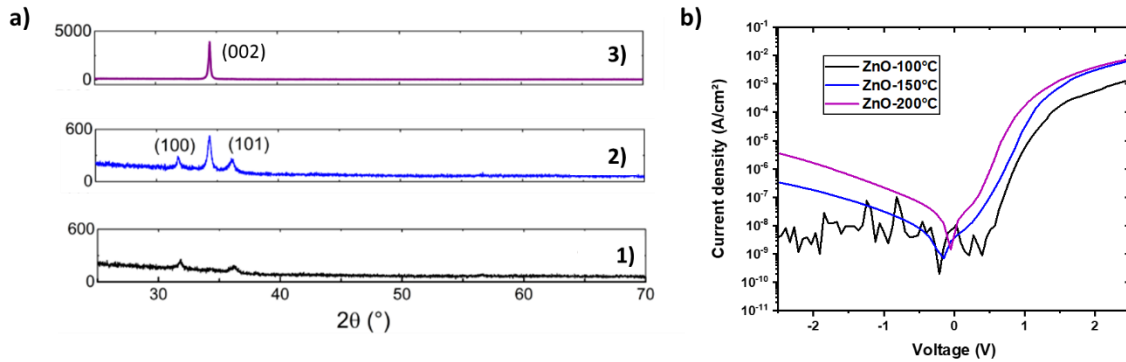


Figure 2. Effect of the deposition temperature of ZnO by AP-SALD a) XRD patterns of the ZnO layers deposited at 1) 100°C, 2) 150°C, and 3) 200°C, adapted by the Nguyen Ph.D. thesis⁶⁵. b) Effect of the deposition temperature of ZnO over the J-V characteristics of the device when combined with CuCrO₂:70%. The number of ALD cycles was adapted to obtain a 60 nm film, at each temperature

The structural, morphological, optical and compositional properties of the optimized architecture, ITO/CuCrO₂:70%/ZnO-100°C-320 cycles were analysed. Raman spectroscopy was employed to probe the phonon modes of the ITO/CuCrO₂:70% and ITO/CuCrO₂:70%/ZnO structures, Figure 3.a).1) and 3.a).2), respectively. CuCrO₂:70% presents modes at 99 cm⁻¹, 108 cm⁻¹, 149 cm⁻¹, 216 cm⁻¹, and 649 cm⁻¹. The Raman mode at 99 cm⁻¹ is attributed to the E_u mode of the CuCrO₂ phase, while the further modes are assigned to the Cu₂O phase, which present more active Raman modes than the delafossite one²⁹. This demonstrates the deposition of a nanocomposite composed of Cu₂O+CuCrO₂, as expected from our previous results²⁹. The additional broad and badly formed Raman mode in the 500-600 cm⁻¹ is attributed to the ITO substrate. The Raman spectrum for the complete device is reported in Figure 3.a).2). The additional Raman lines found at 90 cm⁻¹ and 439 cm⁻¹ are assigned to the E₂^{low} and E₂^{high} modes of the ZnO wurtzite structure, respectively.

GIXRD has been used to confirm these results. The pattern of the ITO substrate, Figure 3.b).1), is reported as comparison. We can observe in Figure 3.b).2) corresponding to ITO/CuCrO₂:70% sample the peaks at 31.9° and 65,3° attributed to the (012) and the (00 $\bar{1}$ 2) reflections of the delafossite; the remaining peaks are attributed to the ITO substrate. The GIX RD pattern of the optimized p-n junction is reported in Figure

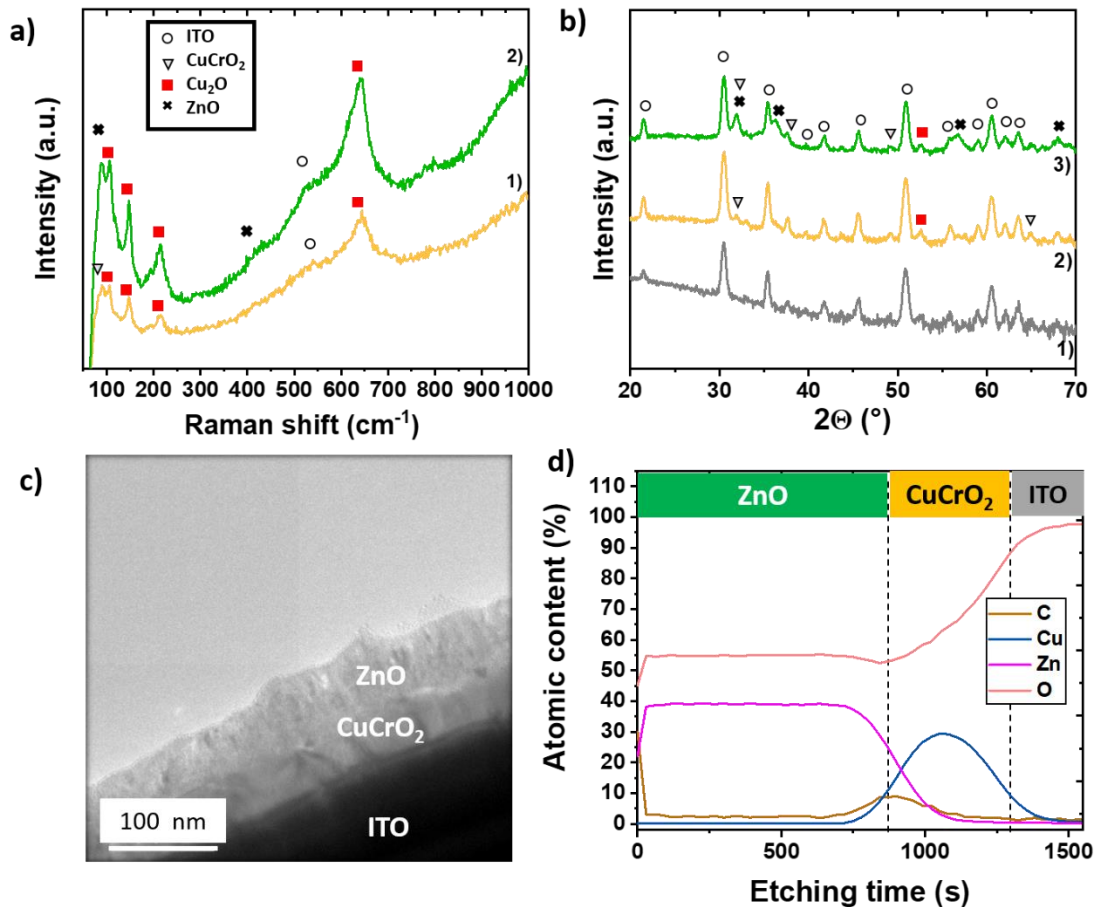


Figure 3. Structural, morphological and optical properties of the optimized structure composed by CuCrO₂:70% and polycrystalline ZnO. b) Raman spectra of 1) ITO/CuCrO₂:70% and 2) p-n junction. b) GIXRD patterns of 1) ITO covered glass, 2) ITO/CuCrO₂:70% and 3) ITO/CuCrO₂:70%/ZnO-100°C-320 cycles. The legend in figure 3.a) is valid also in b). c) TEM cross section of the optimized architecture p-n junction. d) atomic content depth profile as a function of the etching time acquired by XPS for the same sample.

3.b).3). Additional peaks at 31.7° , 36.2° , 56.6° , and 67.9° are attributed to the (100), (101), (110), and (112) reflections of the ZnO wurtzite phase respectively. The polycrystalline nature of this film is in good agreement with previous results obtained for the ZnO seed layers used to grow ZnO nanowires². SAED pattern of the optimized device, figure S4), confirmed the results obtained by XRD.

Cross-section TEM observations were employed to measure the thickness of the films, as shown in Figure 3.c). The device is composed of 30 ± 5 nm of CuCrO_2 film and 60 ± 10 nm for ZnO.

The in-depth profile of the atomic content (C, Cu, Zn and O) of the optimized p-n junction, analyzed by XPS, is represented as a function of the etching time in Figure 3.d). The interface is found after around 900 s of sputtering. The signal of $\text{Cr}_{2p_{3/2}}$ orbital is not reported because it overlapped the one of Zn Auger, in the 580-590 eV range. One can observe a small region, around the interface, where both Zn and the Cu are present. However, we attributed this overlapping to the accuracy of the technique and the fact that our films are very thin, rather than inter-layer diffusion. Finally, this profile allows us to conclude that our layers are chemically stable and no interdiffusion occurs among them, thanks to the low deposition temperature used for the synthesis of ZnO. This is in agreement with the results obtained for the $\text{Cu}_{0.66}\text{Cr}_{1.33}\text{O}_2/\text{ZnO}$ junctions, where the authors demonstrated that even after annealing at 700°C , the layer would not interdiffuse⁵⁴. Furthermore, we can observe a clear accumulation of carbon contamination at the interface, which can be considered the responsible for the shift of our curve with respect to the zero-bias. The evolution of the spectra for the various elements as a function of the etching time is reported in **Erreur ! Source du renvoi introuvable.**

The transmittance spectra for each fabrication step of the device are reported in Figure 4.a). The average optical transmittance in the 400-800 nm range increases from around 60% for the ITO/ CuCrO_2 :70% structure up to 75% for the finalized device. This increase suggests that the ZnO film works as an antireflective coating, mitigating the reflectivity of the CuCrO_2 . Similar values of transparency were obtained by Wang et al.³² for ITO/ CuCrO_{2+x} /ZnO structure.

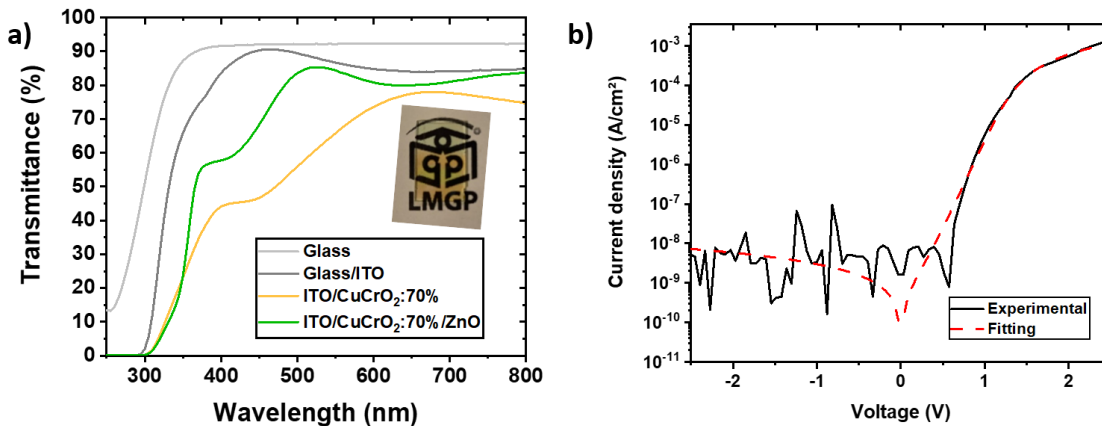


Figure 4. a) Comparison between transmittance spectra of ITO, ITO/ CuCrO_2 :70%, and ITO/ CuCrO_2 :70%/ZnO. The spectrum of the glass substrate is reported for comparison. The inset shows the macroscopic aspect of the device, before the deposition of the gold contacts. b) Fitting of the ITO/ CuCrO_2 :70%/ZnO device characteristics.

The J-V characteristic of the optimized device was fitted, and the results are reported in Figure 4.b). The turn-on voltage was obtained from the linear fit of the J-V characteristic in linear scale, Figure S4. The obtained values for the threshold voltage, the ideality factor η , the series resistance, and the shunt resistance were 0.85 V, 3.9, $850 \Omega \cdot \text{cm}^{-2}$, and $350 \text{M}\Omega \cdot \text{cm}^{-2}$, respectively.

Figure 5 shows the energetic level of the different layers and the resulting band diagram for the optimized p-n junction, Figure 5.a) and Figure 5.b), respectively. The electronic affinity was obtained from the literature, with values around 4.7 eV⁶¹ for ITO, 2.1 eV⁵⁴ for CuCrO₂, 4.3 eV⁶² for ZnO, and 5.1 eV⁶³ for Au. In the case of CuCrO₂, we assume that these values were not significantly influenced by the variation in stoichiometry. For the n-type TCO, this value was previously used by Afonso et al.⁵⁴ for ZnO deposited at 150 °C by ALD, thus we consider it applicable in our case as well. These values indicate a type-II alignment between the CuCrO₂ and ZnO.

The energy gap values were extracted from our previous works, as reported in Table 1. with values of 2.9 eV⁵⁷ and 3.4 eV⁴⁸ for the CuCrO₂ and ZnO, respectively. The position of the Fermi level for Cu₂O+CuCrO₂ was obtained in our previous work²⁹, assuming a similar valence band structure for CuCrO₂:60%, and the CuCrO₂:70%, with values around 70 meV, above the valence band maximum (VBM). This is in good agreement with the extremely high carrier density for the delafossite. Furthermore, the formation of a secondary phase can lead to the formation of quasi-Fermi levels between the VBM and the Fermi energy. Thus, the out of stoichiometry CuCrO₂ is very likely to present a broadening of the bands with less localized states close to the VBM. For ZnO, the low crystallinity and the short-range order, as demonstrated by XRD and SAED, would imply a broadening of the band edges into tails of localized states.

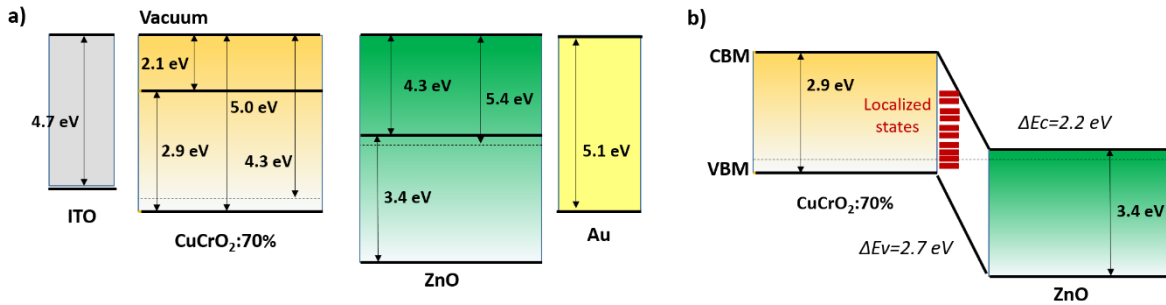


Figure 5. a) Proposed energetic levels of each material prior the contact. The values were obtained by the references and Tauc plot. b) Band diagram for the p-n junction based on CuCrO₂:70% and ZnO. Here, the interface states are evidenced.

The performance of our devices were compared with those in the literature for p-n junctions based on the same materials, Figure 6. Based on this comparison, we can assert that our optimized device presents the highest rectifying ratio ever reported, 3 orders of magnitude greater than what is present in the literature. Moreover, they are characterized by very high transparency, around 75% in the visible range, one of the highest for these devices. These findings highlight that our devices are excellent candidates for highly-performant transparent p-n junctions.

4. Discussion

In this work, p-CuCrO₂/n-ZnO diodes were fabricated and analysed. First, an optimization of the composition of the p-type oxide grown by AAMOCVD was carried on, while the ZnO top layer was always deposited at 100°C by AP-SALD. These devices are labelled CuCrO₂:X, where X represent the cationic ratio i.e. Cu/(Cu+Cr) in the solution employed to synthesize the p-type semiconductors. From these results, Figure 1, we can observe that films with solution composition of 70% correspond to the best candidate, with a value of Ion/Ioff (±2.5V) around 10⁵.

The greater performances of CuCrO₂:70% can be explained through the simultaneous enhancement of the crystallization for the 70% film and the improvement of the transport properties. Indeed, if one supposes only a reduction of the energy gap with the out-stoichiometry, Table 2, one should expect that the CuCrO₂:60% would present a greater rectification ratio than the 70%. However, this is not observed suggesting that other parameters play a more significant role over the performances of the device. As explained by Lim et al.⁵⁶, the increase of the reverse current implies the presence of current leakage paths through deep defects states at the interface, whose density would be reduced by a greater crystallinity of the films. Based on these considerations, it can be expected that the CuCrO₂:70%, which possesses a greater crystallinity than the CuCrO₂:60% film as proved by our previous work²⁹, presents a lower reverse current, i.e., greater rectification ratio than the CuCrO₂:60%. The same applies when increasing the % of Cu from 70% to 80%, i.e. a degradation of the transport properties yields a lower performance of the diode. In our previous work⁵⁷, we demonstrated that the stoichiometry of the films results in a negligible effect over the roughness of the films, thus we exclude that the evolution of I_{on}/I_{off} found for increasing cationic ratio would be related to a significant change in morphology. However, also the transport properties of the film, Table 1, play an important role in the final device performance, tuning, for instance, the depletion region width. Moreover, we cannot exclude the rise of the interband gap state through the formation of Cu₂O for the nanocomposite films which occurs at 70% solution composition.

Based on these results, CuCrO₂:70% was selected to further improve the devices by optimizing the n-type

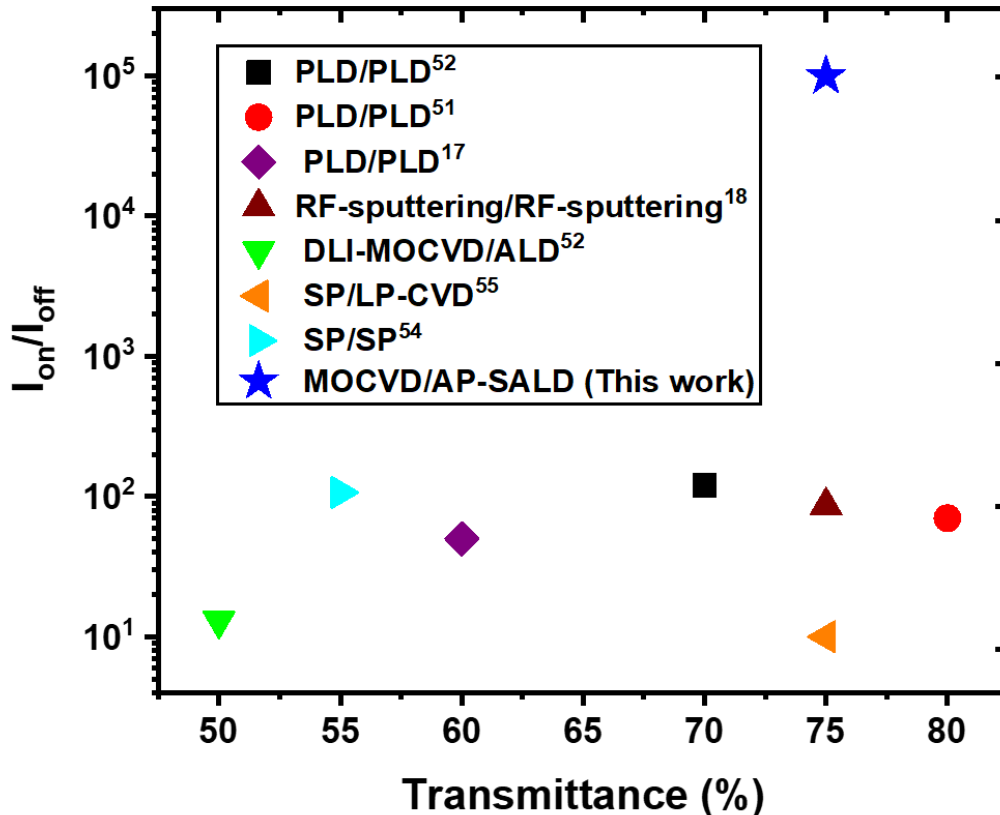


Figure 6. Rectification ratio, I_{on}/I_{off} , as a function of the average transmittance in the visible for CuCrO₂/ZnO based heterojunctions, as obtained by literature. Each work is labelled based on the deposition technique used for the CuCrO₂ and ZnO synthesis

ZnO layer deposited by AP-SALD. In particular, the effect of deposition temperatures for ZnO over the

performances of the diodes was analysed in Figure 2. The forward bias current exceeds the reverse bias current by two orders of magnitude for the three deposition temperatures. As mentioned before, a higher deposition temperature would lead to an increase in the film crystallinity and electrical conductivity. The increase in reverse current corresponds to the main cause of the deteriorated rectification ratio. While this may sound contradictory with the discussion above for CuCrO_2 , one has to take into account the possible different evolution of the interface at the different ZnO deposition temperatures. Indeed, Chiu et al.⁵² reported devices with inverted architecture, namely, $\text{ZnO}/\text{CuCrO}_2:\text{Mg}$ and observed that a greater deposition temperature for the top layer deposition and the large lattice mismatch of the used n- and p-type semiconductor may induce defects at the interface and at the grain boundaries resulting in an increasing leakage current. This will complicate the correlation between the properties of the top layer (ZnO in our case) and the diode performances. In our case, we can suppose that the poor crystallinity of the ZnO deposited at 100 °C may minimize the leakage paths through grain boundaries thus resulting in a limited reverse current, contrarily to what observed for diodes where ZnO was deposited at a temperature higher than 100 °C.

The greatest performances were obtained for the combination of CuCrO_2 synthesized by X=70% and a 60 nm thick ZnO film deposited at 100 °C, summarized as $\text{ITO}/\text{CuCrO}_2:70\%/\text{ZnO-100}^\circ\text{C-320 cycles}$. These heterojunctions were further characterized. GI-XRD and Raman spectroscopy demonstrated the deposition of a nanocomposite $\text{Cu}_2\text{O}+\text{CuCrO}_2$ and of a ZnO wurtzite structure. XPS profiling evidences no significant interdiffusion of the cations and the presence of carbon contamination at the interface, which can be explained through the exposure of CuCrO_2 to open-air between the two deposition processes. Based on this we can forecast the amelioration of the performance through a greater cleaning of the interface before the deposition of the ZnO.

Two main parameters extrapolated by the fitting of the experimental curves are here discussed, the ideality factor and the threshold voltage.

The found ideality factor, 3.9, is coherent with previous reports of all oxides-based diodes, where the typical value is greater than 2^{2,54,64}. Only recently, Narro et al.⁵⁵ reported a similar junction with a value of η as low as 1.57. In our case, the value of η can indicate the presence of additional recombination processes in addition to the Shockley–Read–Hall recombination phenomena. It is our belief that the majority of these recombination center is located at the interface among the semiconductors. The formation of such defects at the interface is likely attributed to the presence of adventitious carbon at the surface of the p- CuCrO_2 , its deviation from stoichiometry and the appearance of the cuprous oxides in the lattice matrix. The latter may represent a further degree of crystalline disarrange. All these factors may result in the arise of intraband states, justifying the discrepancy with the ideal diode. However, the proper definition of their origin and energetic levels will be subject of further studies.

Similar hypotheses were proposed by Afonso et al.⁵⁴, to explain the found value for ideality factor of 6.6, for diodes with a similar structure, $\text{Cu}_{0.66}\text{Cr}_{1.33}\text{O}_2/\text{ZnO}$. The authors attributed their relatively high values to the formation of mid-gap impurity levels active as localized states induced by a high interface defect density or the chromium excess. The parasitic resistance values are influenced by different factors, such as the electrical properties of the thin films, the quality of the interfaces, and defects generated during fabrication. Thus, any speculation about these values may lead to improper conclusions. The fitted values suggest a great quality of the $\text{CuCrO}_2:70\%/\text{ZnO}$ planar heterostructure obtained here. Nevertheless, it can be observed that the experimental characteristic does not pass through the origin, differently by the fitting curve. As explained above, this can be justified by the presence of defects at the interface, which may act as dipoles thus resulting in accumulation of the charges, resulting in a shift of the curves. This may also suggest that the junction may show a hysteresis in the J-V curves, acting as piezoelectric or ferro electric material, finally

appealing for memory applications. Nevertheless, this study was considered for future analysis and it is has not been investigated by our group so far.

The threshold voltage should correspond to the difference in energy of the VBM of the p-type semiconductor and the conduction band minimum of the n-type one. In our case we estimated a value of ΔE_c , around 2.2 eV, while we obtained a turn-on voltage, around 0.85 eV. This suggests the presence of interfacial states, similar to the results reported by Afonso et al.⁵⁴. The authors explain that the presence of defects states at the interface can justify the lower voltage necessary to flatten the bands when compared to the energetic difference between the conduction bands. In our case, the presence of a high interface defect density can be explained by the formation of the Cu_2O secondary phase, the Cu excess of the p-type TCO side, and the poor crystallinity of the ZnO. These factors will result in the broadening of the bands with the formation of midgap levels, allowing the carrier conduction even with a lower amount of energy. The presence of these intrabands levels can justify the high performances and the high ideality factor for our devices.

Our fabrication process presents various advantages.

- i) First, we successfully fabricated our devices through relatively rapid and scalable methods.
- ii) Second, we employed the lowest deposition temperature ever reported for this type of thin films ($T_{\text{max}} 350^\circ\text{C}$), without the use of vacuum techniques or additional post annealing treatments.
- iii) Furthermore, the results presented are achieved without the use of extrinsic dopant, for none of our layers. This represents an additional advantage since it makes our manufacturing process less sophisticated than the many reports previously reported.
- iv) Finally, all these factors will contribute to the reduction of costs and time for the production of high-performance p-n planar heterojunctions, thus resulting an extremely appealing factor for the industrialization of such technology.

These results highlight the feasibility of the proposed oxides as promising semiconductors for transparent heterojunctions, revealing great performance of the devices as well as an auspicious route to fabricate them.

5. Conclusions

We reported high-performance diodes based on ZnO and on out of stoichiometry CuCrO_2 fabricated by chemical deposition methods at low temperature and ambient pressure, without the requirement of any further post-deposition treatment. After a selection of various deposition parameters, the architecture was optimized, resulting in an ITO/ $\text{CuCrO}_2:70\%/\text{ZnO}$. The diodes prepared in this work present the highest rectification ratio reported in the literature, with mean values around 10^5 . The reproducibility of these results was confirmed. These extremely high performances are attributed to the formation of intraband levels, due to the stoichiometry variation of the CuCrO_2 phase and the poor crystallinity of n-type ZnO deposited at low temperature, 100°C . Moreover, these devices are characterized by very high transparency in the visible range, around 75%, due to the antireflective properties of the ZnO thin films. These encouraging results and the upscaling possibilities are extremely appealing for the industrialization of such transparent and oxide-based devices.

6. Acknowledgments

L. Bottiglieri acknowledges the French Ministry of Higher Education and Research for funding his PhD scholarship. This research has benefited from the characterization equipment of the Grenoble INP – CMTC platform supported by the Centre of Excellence of Multifunctional Architected Materials “CEMAM” noANR-10-LABX-44-01 funded by the “Investments for the Future” Program. This work benefited from the facilities and expertise of the (OPE)N(RA characterization platform of the FMNT (FR 2542)) supported by CNRS, Grenoble INP and UGA. The authors would like to warmly acknowledge Laetitia Rapenne for the help on TEM observations and Hervé Roussel for the aid on the GI-XRD pattern acquisition. Agence Nationale de la Recherche (ANR) is acknowledged for financial support under contracts ANR-16-CE05-0021 (DESPATCH) and ANR-15-IDEX-02 (Eco-SESA).

7. Bibliography

1. Zhai, T. *et al.* A comprehensive review of one-dimensional metal-oxide nanostructure photodetectors. *Sensors* **9**, 6504–6529 (2009).
2. Cossuet, T. *et al.* ZnO/CuCrO₂ Core–Shell Nanowire Heterostructures for Self-Powered UV Photodetectors with Fast Response. *Adv. Funct. Mater.* **28**, 1–12 (2018).
3. Fortunato, E., Barquinha, P. & Martins, R. Oxide Semiconductor Thin-Film Transistors: A Review of Recent Advances. *Adv. Mater.* **24**, 2945–2986 (2012).
4. Granqvist, C. G. Transparent conductors as solar energy materials: A panoramic review. *Sol. Energy Mater. Sol. Cells* **91**, 1529–1598 (2007).
5. Kim, G. *et al.* Transparent Thin-Film Silicon Solar Cells for Indoor Light Harvesting with Conversion Efficiencies of 36% without Photodegradation. *ACS Appl. Mater. Interfaces* **12**, 27122–27130 (2020).
6. Liu, H., Avrutin, V., Izyumskaya, N., Özgür, Ü. & Morkoç, H. Transparent conducting oxides for electrode applications in light emitting and absorbing devices. *Superlattices Microstruct.* **48**, 458–484 (2010).
7. Yim, K. *et al.* Computational discovery of p-type transparent oxide semiconductors using hydrogen descriptor. *npj Comput. Mater.* **4**, 17 (2018).
8. Abdelfatah, M. *et al.* Fabrication and characterization of low cost Cu₂O/ZnO:Al solar cells for sustainable photovoltaics with earth abundant materials. *Sol. Energy Mater. Sol. Cells* **145**, 454–461 (2016).
9. Sato, H., Minami, T., Takata, S. & Yamada, T. Transparent conducting p-type NiO thin films prepared by magnetron sputtering. *Thin Solid Films* **236**, 27–31 (1993).
10. Sekkat, A. *et al.* Open-air printing of Cu₂O thin films with high hole mobility for semitransparent solar harvesters. *Commun. Mater.* **2**, 1–10 (2021).
11. Nguyen, V. S. *et al.* Open-air, low-temperature deposition of phase pure Cu₂O thin films as efficient hole-transporting layers for silicon heterojunction solar cells. *J. Mater. Chem. A* **9**, 15968–15974 (2021).
12. Steirer, K. X. *et al.* Solution deposited NiO thin-films as hole transport layers in organic photovoltaics. *Org. Electron.* **11**, 1414–1418 (2010).
13. Resende, J., Jiménez, C., Nguyen, N. D. & Deschanvres, J. L. Magnesium-doped cuprous oxide

- (Mg:Cu₂O) thin films as a transparent p-type semiconductor. *Phys. Status Solidi Appl. Mater. Sci.* **213**, 2296–2302 (2016).
14. Kaya, I. C., Akin, S., Akyildiz, H. & Sonmezoglu, S. Highly efficient tandem photoelectrochemical solar cells using coumarin6 dye-sensitized CuCrO₂ delafossite oxide as photocathode. *Sol. Energy* **169**, 196–205 (2018).
 15. Kavan, L. Electrochemistry and dye-sensitized solar cells. *Curr. Opin. Electrochem.* **2**, 88–96 (2017).
 16. Tripathi, T. S., Niemelä, J.-P. & Karppinen, M. Atomic layer deposition of transparent semiconducting oxide CuCrO₂ thin films. *J. Mater. Chem. C* **3**, 8364–8371 (2015).
 17. Chiu, T., Tonooka, K. & Kikuchi, N. Preparation of transparent p-CuCrO₂:Mg/n-ZnO heterojunction with in situ laser annealing. *SAW Futur. Mob. Comm. Syst.* 2–4 (2004).
 18. Chen, L.-F., Wang, Y.-P., Chiu, T.-W., Shih, W.-C. & Wu, M.-S. Fabrication of Transparent CuCrO₂:Mg/ZnO p-n Junctions Prepared by Magnetron Sputtering on an Indium Tin Oxide Glass Substrate. *Jpn. J. Appl. Phys.* **52**, 05EC02 (2013).
 19. Crépellière, J. *et al.* Transparent conductive CuCrO₂ thin films deposited by pulsed injection metal organic chemical vapor deposition: Up-scalable process technology for an improved transparency/conductivity trade-off. *J. Mater. Chem. C* **4**, 4278–4287 (2016).
 20. Lunca Popa, P., Crépellière, J., Leturcq, R. & Lenoble, D. Electrical and optical properties of Cu-Cr-O thin films fabricated by chemical vapour deposition. *Thin Solid Films* **612**, 194–201 (2016).
 21. Mahapatra, S. & Shivashankar, S. A. Low-pressure metal-organic CVD of transparent and p-type conducting CuCrO₂ thin films with high conductivity. *Chem. Vap. Depos.* **9**, 238–240 (2003).
 22. Farrell, L. *et al.* Spray pyrolysis growth of a high figure of merit, nano-crystalline, p-type transparent conducting material at low temperature. *Appl. Phys. Lett.* **107**, 2–7 (2015).
 23. Farrell, L. *et al.* Synthesis of nanocrystalline Cu deficient CuCrO₂ – a high figure of merit p-type transparent semiconductor. *J. Mater. Chem. C* **4**, 126–134 (2016).
 24. Chikoidze, E. *et al.* Control of p-type conduction in Mg doped monophase CuCrO₂ thin layers. *J. Phys. D. Appl. Phys.* **49**, 205107 (2016).
 25. Sánchez-Alarcón, R. I. *et al.* Ultrasonic spray-pyrolyzed CuCrO₂ thin films. *J. Phys. D. Appl. Phys.* **49**, 175102 (2016).
 26. Götzendörfer, S. & Löbmann, P. Influence of single layer thickness on the performance of undoped and Mg-doped CuCrO₂ thin films by sol-gel processing. *J. Sol-Gel Sci. Technol.* **57**, 157–163 (2011).
 27. Götzendörfer, S., Polenzky, C., Ulrich, S. & Löbmann, P. Preparation of CuAlO₂ and CuCrO₂ thin films by sol-gel processing. *Thin Solid Films* **518**, 1153–1156 (2009).
 28. Jeong, S., Seo, S. & Shin, H. P-Type CuCrO₂ particulate films as the hole transporting layer for CH₃NH₃PbI₃ perovskite solar cells. *RSC Adv.* **8**, 27956–27962 (2018).
 29. Bottiglieri, L. *et al.* Out of stoichiometry CuCrO₂ films as a promising p-type TCO for transparent electronics. *Mater. Adv.* **2**, 4721–4732 (2021).
 30. Sidik, U., Kim, J. H., Kim, H.-K., Lee, H. Y. & Lee, J. Structures and characteristics of delafossite CuCr_{1-x}O₂ thin films prepared by pulsed laser deposition. *Micro Nano Lett.* **9**, 854–857 (2014).

31. Lunca-Popa, P. *et al.* Tuning the electrical properties of the p-type transparent conducting oxide $\text{Cu}_{1-x}\text{Cr}_{1+x}\text{O}_2$ by controlled annealing. *Sci. Rep.* **8**, 1–8 (2018).
32. Wang, J. *et al.* Combustion Synthesis of p-Type Transparent Conducting CuCrO_{2+x} and $\text{Cu}:\text{CrO}_x$ Thin Films at 180 °C. *ACS Appl. Mater. Interfaces* **10**, 3732–3738 (2018).
33. Zhang, H. *et al.* Low-Temperature Solution-Processed CuCrO_2 Hole-Transporting Layer for Efficient and Photostable Perovskite Solar Cells. *Adv. Energy Mater.* **8**, (2018).
34. Gil, B. *et al.* CuCrO_2 nanoparticles incorporated into PTAA as a hole transport layer for 85°C and light stabilities in perovskite solar cells. *Nanomaterials* **10**, 1–13 (2020).
35. Dimple, D., Lebègue, S. & Pastore, M. Dye Anchoring on CuCrO_2 Surfaces for p-Type Dye-Sensitized Solar Cell Applications: An Ab Initio Study. *ACS Appl. Energy Mater.* acaem.1c00970 (2021) doi:10.1021/acsaem.1c00970.
36. Xiong, D. *et al.* Hydrothermal synthesis of ultrasmall CuCrO_2 nanocrystal alternatives to NiO nanoparticles in efficient p-type dye-sensitized solar cells. *J. Mater. Chem.* **22**, 24760–24768 (2012).
37. Cossuet, T. *et al.* ZnO/ CuCrO_2 Core–Shell Nanowire Heterostructures for Self-Powered UV Photodetectors with Fast Response. *Adv. Funct. Mater.* **28**, 1–12 (2018).
38. Ahmadi, M., Abrari, M. & Ghanaatshoar, M. An All-sputtered Photovoltaic Ultraviolet Photodetector Based on Co-doped CuCrO_2 and Al-doped ZnO Heterojunction. *Sci. Rep.* **11**, 1–10 (2021).
39. Li, Y. *et al.* A Solution-Processed Hole-Transporting Layer Based on p-Type CuCrO_2 for Organic Photodetector and Image Sensor. *Adv. Mater. Interfaces* **2100801**, 2100801 (2021).
40. Tong, B. *et al.* Oxygen vacancy defects boosted high performance p-Type delafossite CuCrO_2 gas sensors. *ACS Appl. Mater. Interfaces* **10**, 34727–34734 (2018).
41. Zhou, S. *et al.* Room temperature ozone sensing properties of p-type CuCrO_2 nanocrystals. *Sensors Actuators, B Chem.* **143**, 119–123 (2009).
42. Creissen, C. E. *et al.* Inverse Opal CuCrO_2 Photocathodes for H_2 Production Using Organic Dyes and a Molecular Ni Catalyst. *ACS Catal.* **9**, 9530–9538 (2019).
43. Xu, Y. *et al.* Enhancing Q-Switched Fiber Laser Performance Based on Reverse Saturable and Saturable Absorption Properties of CuCrO_2 Nanoparticle-Polyimide Films. *ACS Appl. Mater. Interfaces* **13**, 21748–21755 (2021).
44. Ajimsha, R. S. *et al.* Transparent p-AgCoO₂/n-ZnO diode heterojunction fabricated by pulsed laser deposition. *Thin Solid Films* **515**, 7352–7356 (2007).
45. Siol, S. *et al.* Band Alignment Engineering at $\text{Cu}_2\text{O}/\text{ZnO}$ Heterointerfaces. *ACS Appl. Mater. Interfaces* **8**, 21824–21831 (2016).
46. Giusti, G., Consonni, V., Puyoo, E. & Bellet, D. High performance ZnO-SnO₂:F nanocomposite transparent electrodes for energy applications. *ACS Appl. Mater. Interfaces* **6**, 14096–14107 (2014).
47. Janotti, A. & Van De Walle, C. G. Fundamentals of zinc oxide as a semiconductor. *Reports Prog. Phys.* **72**, (2009).
48. Nguyen, V. H. *et al.* Deposition of ZnO based thin films by atmospheric pressure spatial atomic

- layer deposition for application in solar cells. *J. Renew. Sustain. Energy* **9**, 021203 (2017).
49. Bhachu, D. S., Sankar, G. & Parkin, I. P. Aerosol assisted chemical vapor deposition of transparent conductive zinc oxide films. *Chem. Mater.* **24**, 4704–4710 (2012).
 50. Hoyer, R. L. Z. *et al.* Research Update: Atmospheric pressure spatial atomic layer deposition of ZnO thin films: Reactors, doping, and devices. *APL Mater.* **3**, (2015).
 51. Tonooka, K. & Kikuchi, N. Preparation of transparent CuCrO₂:Mg/ZnO p–n junctions by pulsed laser deposition. *Thin Solid Films* **515**, 2415–2418 (2006).
 52. Chiu, T. W., Tonooka, K. & Kikuchi, N. Fabrication of transparent CuCrO₂:Mg/ZnO p–n junctions prepared by pulsed laser deposition on glass substrate. *Vacuum* **83**, 614–617 (2008).
 53. Liu, H. *et al.* Reaction Pathway of the Hydrothermal Synthesis of AgCuO₂ from in Situ Time-Resolved X-ray Diffraction. *Cryst. Growth Des.* **20**, 4264–4272 (2020).
 54. Afonso, J., Leturcq, R., Popa, P. L. & Lenoble, D. Transparent p-Cu_{0.66}Cr_{1.33}O₂/n-ZnO heterojunction prepared in a five-step scalable process. *J. Mater. Sci. Mater. Electron.* **30**, 1760–1766 (2019).
 55. Narro-Ríos, J. S. *et al.* Spray pyrolysis synthesis of a semi-transparent p-CuCrO₂/n-ZnO heterojunction: Structural, optical, and electrical properties. *Phys. B Condens. Matter* 413426 (2021) doi:10.1016/j.physb.2021.413426.
 56. Lim, S. H., Desu, S. & Rastogi, A. C. Chemical spray pyrolysis deposition and characterization of p-type CuCr_{1-x}Mg_xO₂ transparent oxide semiconductor thin films. *J. Phys. Chem. Solids* **69**, 2047–2056 (2008).
 57. Bottiglieri, L., Nourine, A., Resende, J., Deschanvres, J. & Jim, C. Optimized Stoichiometry for CuCrO₂ Thin Films as Hole Transparent Layer in PBDD4T-2F:PC₇₀BM Organic Solar Cells. *Nanomaterials* 1–15 (2021) doi:https://doi.org/10.3390/nano11082109.
 58. Huong, N. V. *et al.* Impact of precursor exposure on process efficiency and film properties in spatial atomic layer deposition. *Chem. Eng. J.* (2020) doi:10.1016/j.cej.2020.126234.
 59. Muñoz-Rojas, D. & Macmanus-Driscoll, J. Spatial atmospheric atomic layer deposition: A new laboratory and industrial tool for low-cost photovoltaics. *Mater. Horizons* **1**, 314–320 (2014).
 60. de la Huerta, C. A. M. *et al.* Gas-Phase 3D Printing of Functional Materials. *Adv. Mater. Technol.* **5**, 1–8 (2020).
 61. Lee, K. W. *et al.* A two-dimensional DNA lattice implanted polymer solar cell. *Nanotechnology* **22**, (2011).
 62. Tharsika, T., Haseeb, A. S. M. A., Akbar, S. A., Mohd Sabri, M. F. & Hoong, W. Y. Enhanced ethanol gas sensing properties of SnO₂-core/ZnO-shell nanostructures. *Sensors (Switzerland)* **14**, 14586–14600 (2014).
 63. Kumar, B., Kaushik, B. K. & Negi, Y. S. Perspectives and challenges for organic thin film transistors: Materials, devices, processes and applications. *J. Mater. Sci. Mater. Electron.* **25**, 1–30 (2014).
 64. Grundmann, M. *et al.* Oxide bipolar electronics: Materials, devices and circuits. *J. Phys. D. Appl. Phys.* **49**, (2016).
 65. Nguyen, V. H. Development of transparent electrodes by vacuum-free and low cost deposition

methods for photovoltaic. (2019).